Effective photosensitized emission of a Tb(III) complex using a β-diketonate photosensitizer and an oxygen barrier system in a thermally populated triplet state

Kota Inage[a], Mengfei Wang[b,c], Yasuchika Hasegawa[b,c]*, Yuichi Kitagawa[b,c]*

a. Graduate School of Chemical Sciences and Engineering, Hokkaido University, Sapporo 060-8628, Japan.

b. Faculty of Engineering, Hokkaido University, Sapporo 060-8628, Japan.

c. Institute for Chemical Reaction Design and Discovery (WPI-ICReDD), Hokkaido University, Sapporo 001-0021, Japan.

E-mail: y-kitagawa@eng.hokudai.ac.jp; hasegaway@eng.hokudai.ac.jp

Structure

To estimate the coordination geometries of the complexes, we performed continuous shape measure (CShM) using SHAPE.[1–3] The CShM factor S for N atoms coordination was expressed as follows:

$$S = \min \frac{\sum_{i=1}^{N}|Q_i - P_i|^2}{\sum_{i=1}^{N}|Q_i - Q_0|^2} \times 100$$

where Q_i is the position vectors of the coordination atoms, P_i is the position vector of an ideal structure, and Q_0 is the position vector of the center of mass.

Table S1. The CShM factor S for the Tb(III) and Gd(III) complexes.

Entry	S (SAPR)[a]	S (TDH)[b]	S (BTPR)[c]
[Tb(hfa)$_3$(tppo)$_2$]	0.756	1.118	1.558
[Tb(hfa)$_3$(tcpo)$_2$]	1.233	1.504	1.150
[Gd(hfa)$_3$(tppo)$_2$]	0.839	1.086	1.564
[Gd(hfa)$_3$(tcpo)$_2$]	1.296	1.499	1.155

[a] Square antiprism. [b] Trigonal dodecahedron. [c] Bicapped trigonal prism.
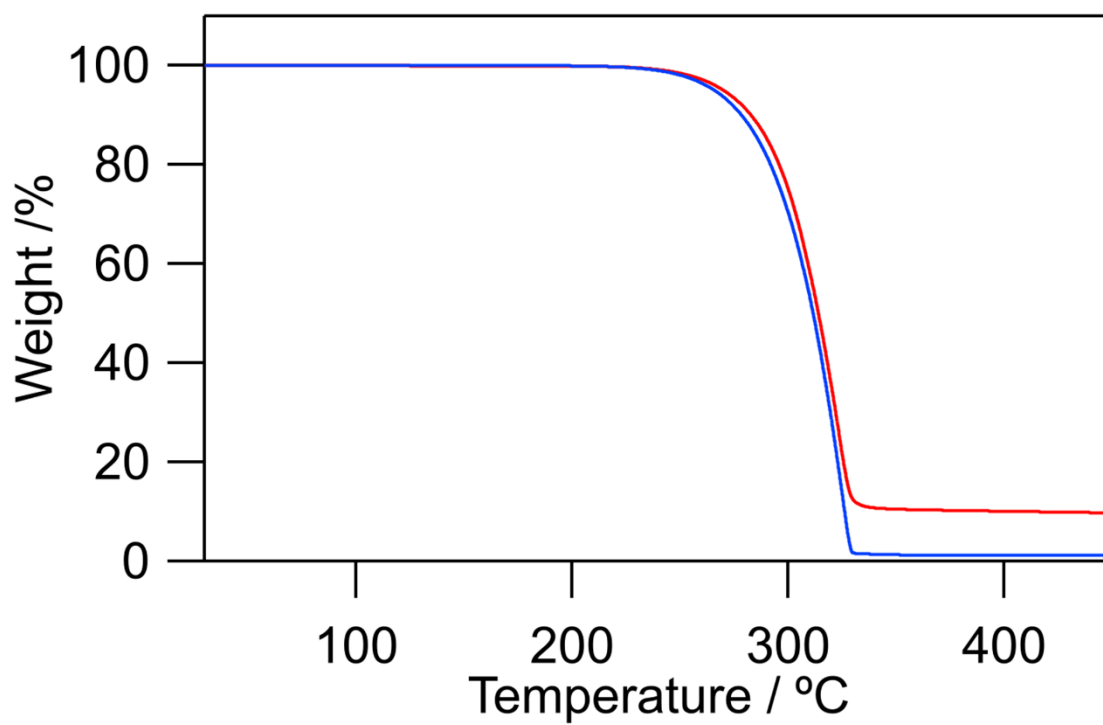
Figure S1. Thermogravimetric analysis profiles of [Tb(hfa)$_3$(tppo)$_2$] (red line) and [Tb(hfa)$_3$(tcpo)$_2$] (blue line) under nitrogen atmosphere at a heating rate of 5°C min^{-1}.

(a)   (b)

SAPR   BTPR
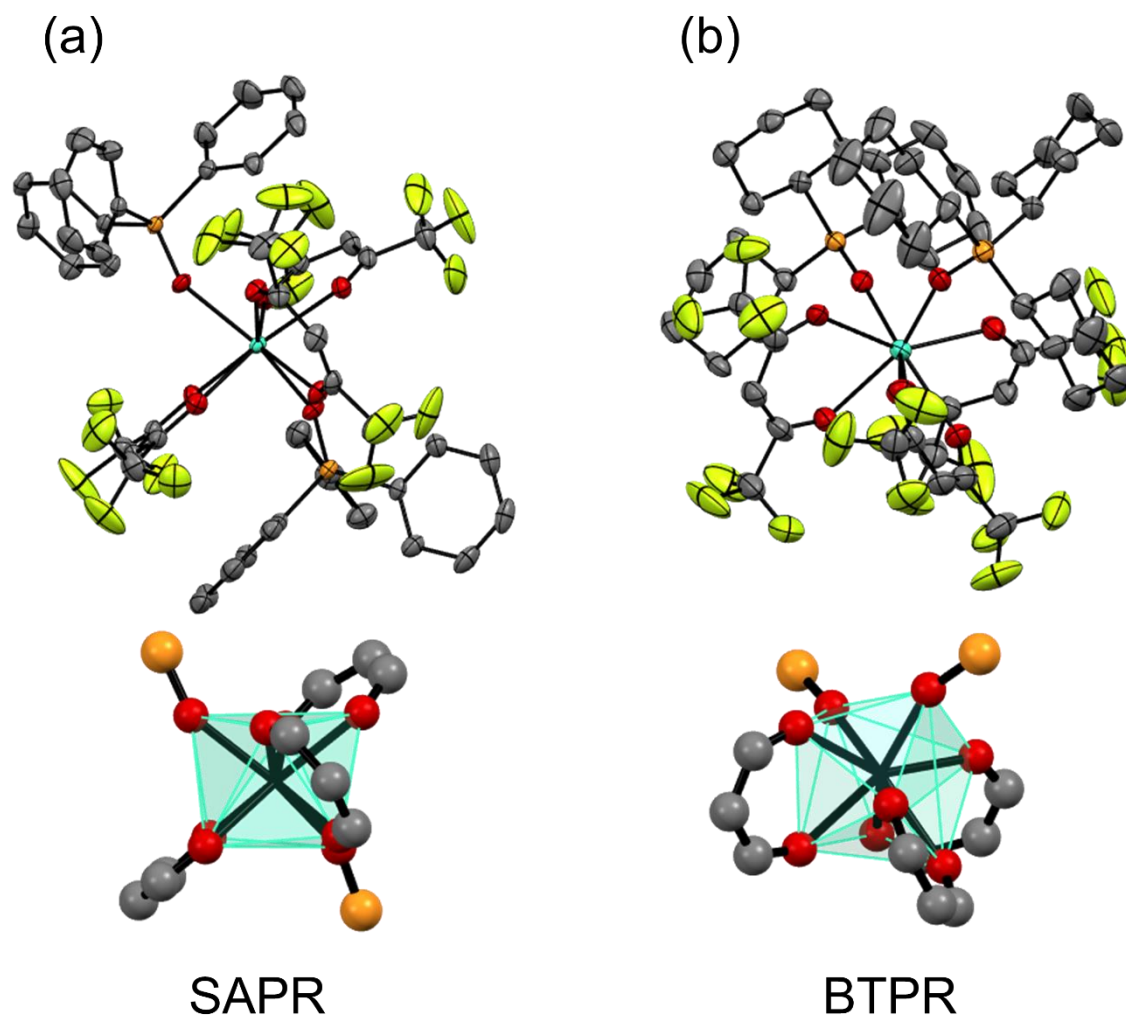
Figure S2. ORTEP drawings (top) and coordination geometries (bottom) of the Gd(III) complexes: (a) [Gd(hfa)$_3$(tppo)$_2$], (b) [Gd(hfa)$_3$(tcpo)$_2$]. Ellipsoids probability was set at 50%. Hydrogen atoms are omitted for clarity.

Table S2. Crystal data of [Gd(hfa)$_3$(tppo)$_2$] and [Gd(hfa)$_3$(tcpo)$_2$].

	[Gd(hfa)$_3$(tppo)$_2$]	[Gd(hfa)$_3$(tcpo)$_2$]
Chemical formula	C$_{51}$H$_{33}$F$_{18}$GdO$_8$P$_2$	C$_{51}$H$_{69}$F$_{18}$GdO$_8$P$_2$
Molecular weight	1334.96	1371.25
Crystal system	monoclinic	orthorhombic
Space group	$P2_1/n$	$Pca2_1$
a / Å	17.0506(4)	17.8798(6)
b / Å	15.4096(3)	18.7861(6)
c / Å	20.5780(5)	17.3285(5)
α / °	90	90
β / °	93.800(2)	90
γ / °	90	90
Volume / Å^3	5394.8(2)	5820.5(3)
Z	4	4
Density / g cm^{-1}	1.644	1.565
Temperature / °C	−150	−150
R_1	0.0323	0.0480
wR_2	0.0785	0.1326

Table S3. Tb-O distances of [Tb(hfa)$_3$(tppo)$_2$].

Ligand	Tb–O distance / Å
hfa1	2.401
	2.397
hfa2	2.428
	2.333
hfa3	2.399
	2.339
Avg.	2.383

Table S4. Tb-O distances of [Tb(hfa)$_3$(tcpo)$_2$].

Ligand	Tb–O distance / Å
hfa1	2.428
	2.399
hfa2	2.414
	2.372
hfa3	2.447
	2.378
Avg.	2.407

Estimation of radiative rate constant k_r

The radiative rate constant k_r of a lanthanide(III) ion can be determined using the following Strickler–Berg equation:[4]

$$k_r = 2303 \times \frac{8\pi c n^2 \tilde{v}(2J+1)}{N_A \left(2J^{'}+1\right)} \int \epsilon(\tilde{v}) \mathrm{d}\tilde{v}$$

where c, n, $\tilde{v}$, and N_A denote the light speed, refractive index, wavenumber, and Avogadro constant, respectively. Meanwhile, J and J' are the total angular momentum of the initial and final 4f-electronic states, respectively. However, the emission spectra in the solution state are different from those in the solid state, thus indicating the different electronic structure of the Tb(III) complexes in the solid and solution states (Figure S3). In addition, the signal-to-noise ratio of the absorption spectra in the $^7F_6 \rightarrow {}^5D_4$ transition in Tb(III) is large and thus could not be used to determine the exact k_r value in solution states (Figure S4).
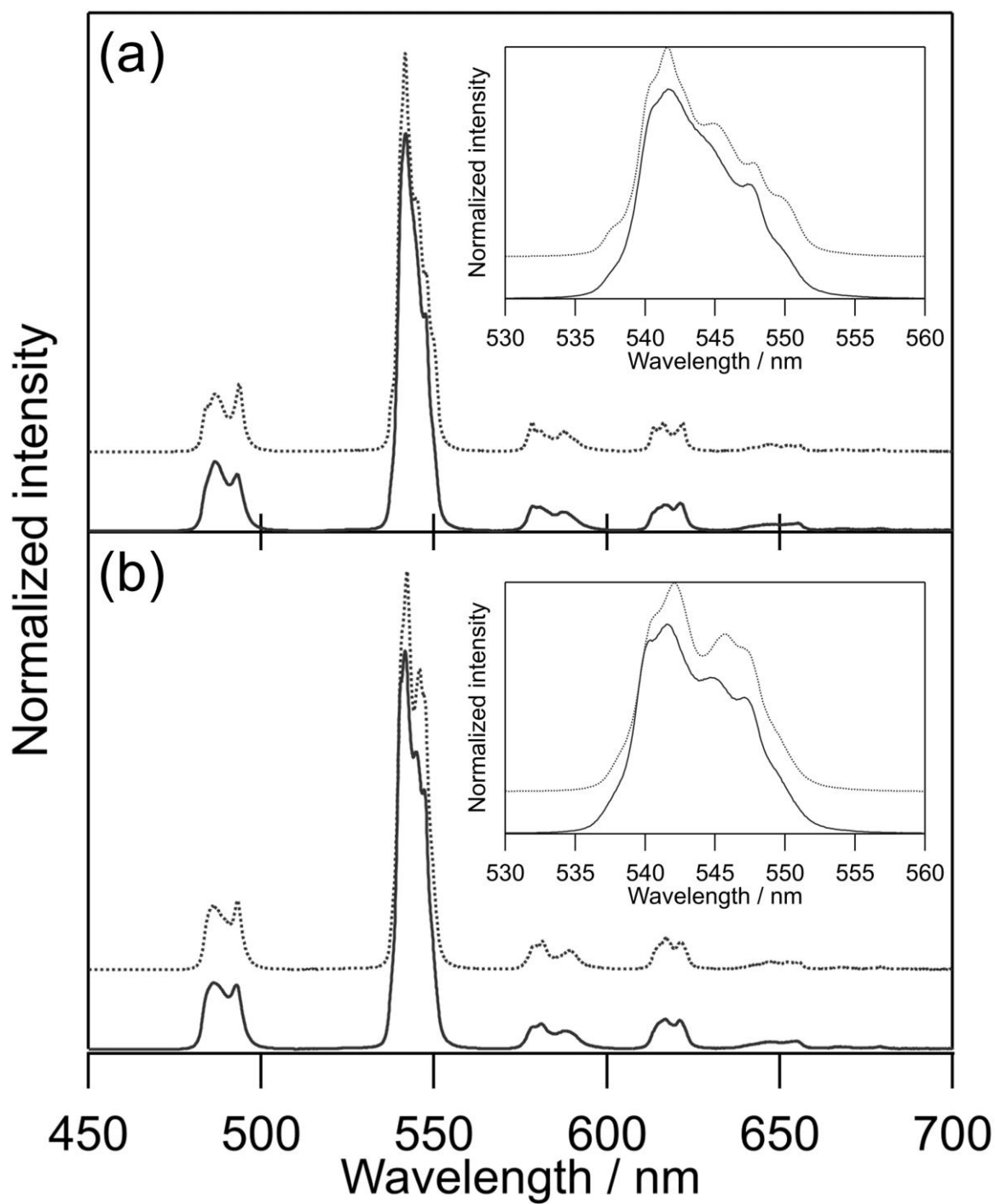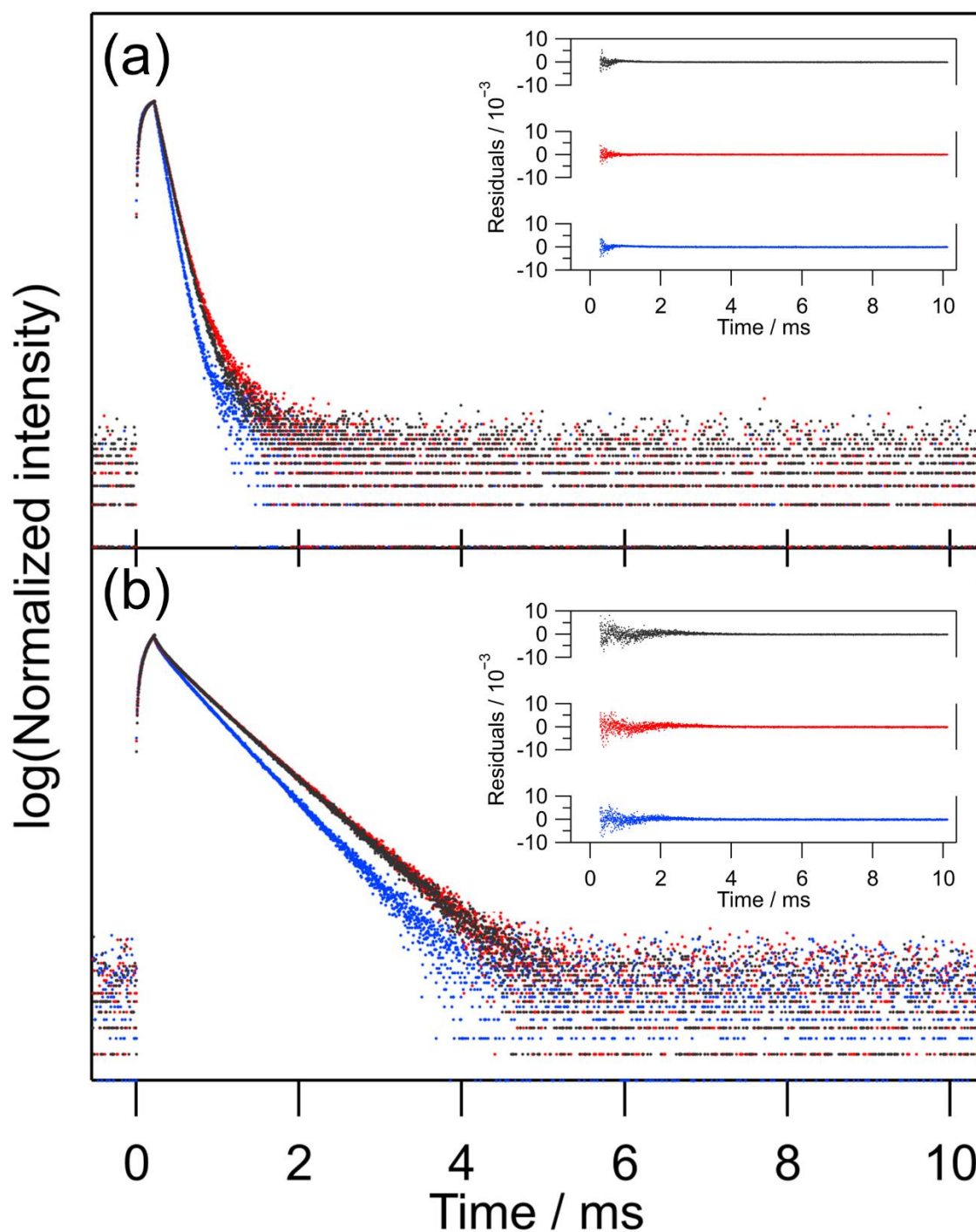
Figure S3. Emission spectra (λ_{ex} = 360 nm, 293 K) of (a) [Tb(hfa)$_3$(tppo)$_2$] and (b) [Tb(hfa)$_3$(tcpo)$_2$] in solid (dotted lines) and solution (solid lines, 1 mM in CHCl$_3$).
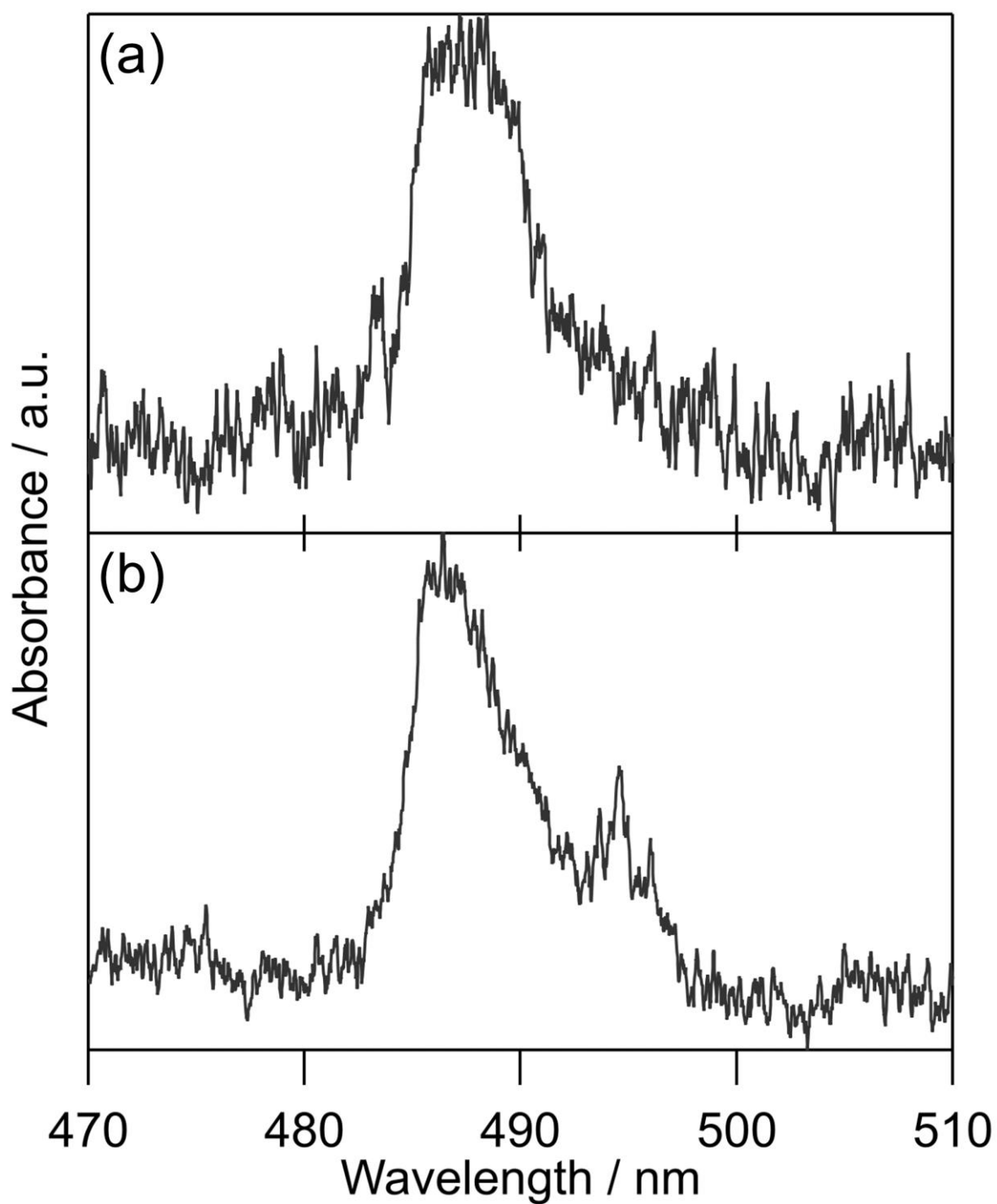
Figure S4. Electronic absorption bands of Tb(III) ions in the Tb(III) complexes: (a) [Tb(hfa)$_3$(tppo)$_2$] (5 mM in CHCl$_3$) and (b) [Tb(hfa)$_3$(tcpo)$_2$] (20 mM in CHCl$_3$) at 293 K.

Figure S5. Emission decay curves (λ_{ex} = 356 nm, λ_{em} = 542 nm, 293 K) of (a) [Tb(hfa)$_3$(tppo)$_2$] and (b) [Tb(hfa)$_3$(tcpo)$_2$] under air (black dots), vacuum (red dots), and O$_2$ (blue dots) conditions (HORIBA Fluorolog-3). The inset figures represent the residuals of double-exponential fitting (Chi-squared test: [Tb(hfa)$_3$(tppo)$_2$]: χ^2 = 0.000378085 (air), 0.000280145 (vacuum), 0.000324166 (O$_2$); [Tb(hfa)$_3$(tcpo)$_2$]: χ^2 = 0.00260252 (air), 0.0025958 (vacuum), 0.00204608 (O$_2$)).

Table S5. Oxygen-concentration dependent emission lifetimes (λ_{ex} = 356 nm, λ_{em} = 542 nm, 293 K) of [Tb(hfa)$_3$(tppo)$_2$]. The average emission lifetimes were obtained through five measurements.

Condition	τ_1 / µs	τ_2 / µs	τ_{avg} / µs
air	93 (86%)	153 (14%)	101
vacuum	98 (96%)	285 (4%)	105
O$_2$	77 (88%)	125 (12%)	82

Table S6. Oxygen-concentration dependent emission lifetimes (λ_{ex} = 356 nm, λ_{em} = 542 nm, 293 K) of [Tb(hfa)$_3$(tcpo)$_2$]. The average emission lifetimes were obtained through five measurements.

Condition	τ_1 / µs	τ_2 / µs	τ_{avg} / µs
air	140 (15%)	507 (85%)	453
vacuum	134 (13%)	515 (87%)	466
O$_2$	116 (11%)	434 (89%)	398
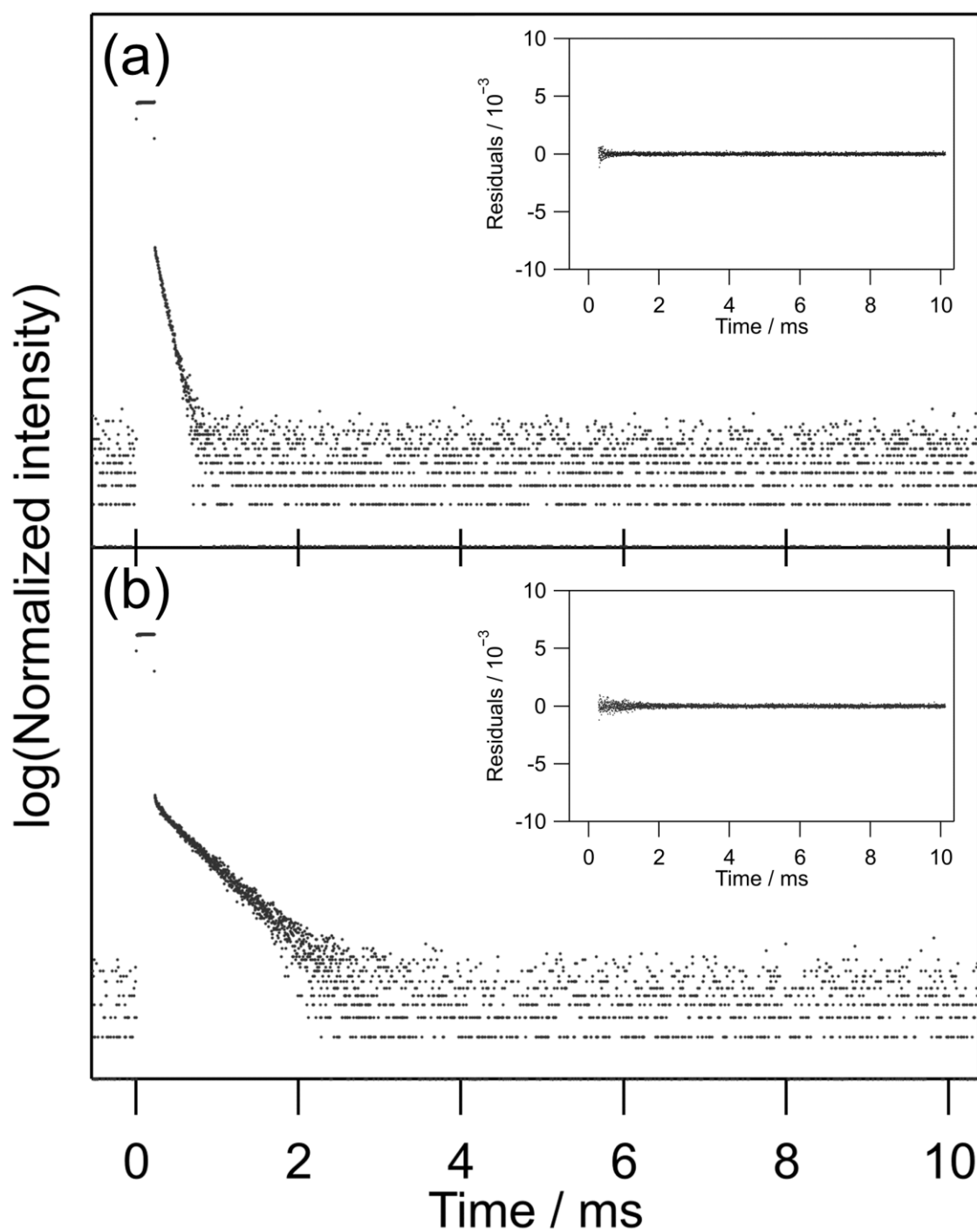
Figure S6. Emission decay curves (λ_{ex} = 495 nm, λ_{em} = 542 nm, 293 K) of (a) [Tb(hfa)$_3$(tppo)$_2$] and (b) [Tb(hfa)$_3$(tcpo)$_2$] under vacuum (HORIBA Fluorolog-3). The inset figures represent the residuals of double-exponential fitting (Chi-squared test: [Tb(hfa)$_3$(tppo)$_2$] χ^2 = 3.16037 × 10^{-6}; [Tb(hfa)$_3$(tcpo)$_2$]: χ^2 = 5.2358 × 10^{-6}).

Table S7. Emission lifetimes (λ_{ex} = 495 nm, λ_{em} = 542 nm, 293 K, under vacuum) of [Tb(hfa)$_3$(tppo)$_2$] and [Tb(hfa)$_3$(tcpo)$_2$]. The average emission lifetimes were obtained through five measurements.

Entry	τ_1 / μs	τ_2 / μs	τ_{avg} / μs
[Tb(hfa)$_3$(tppo)$_2$]	77 (59%)	133 (41%)	99
[Tb(hfa)$_3$(tcpo)$_2$]	84 (10%)	495 (90%)	452

Table S8. Temperature-dependent emission lifetimes (λ_{ex} = 356 nm, λ_{em} = 542 nm, under vacuum) of [Tb(hfa)$_3$(tppo)$_2$].

Temperature / K	Single component	Double components		
	τ_{obs} / μs	τ_1 / μs	τ_2 / μs	τ_{avg} / μs
100	763	-	-	-
150	772	-	-	-
200	742	-	-	-
225	625	-	-	-
250	-	383 (84%)	580 (16%)	414
275	-	203 (92%)	501 (8%)	226
300	-	98 (91%)	297 (9%)	116
350	-	26 (95%)	521 (5%)	49

Table S9. Temperature-dependent emission lifetimes (λ_{ex} = 356 nm, λ_{em} = 542 nm, under vacuum) of [Tb(hfa)$_3$(tcpo)$_2$].

Temperature / K	Single component	Double components		
	τ_{obs} / μs	τ_1 / μs	τ_2 / μs	τ_{avg} / μs
100	894	-	-	-
150	899	-	-	-
200	881	-	-	-
250	-	349 (15%)	858 (85%)	781
275	-	265 (12%)	735 (88%)	681
300	-	183 (16%)	519 (84%)	465
325	-	142 (21%)	497 (79%)	254
350	-	77 (59%)	136 (41%)	101

Arrhenius analysis

To analyze the BEnT properties of the Tb(III) complexes, we performed Arrhenius analysis. Since the back energy transfer doesn't occur at 90 K, the BEnT rate (k_{BEnT}) at each temperature can be expressed as follows:

$$\ln k_{BEnT} = \ln\left(\frac{1}{\tau_{obs}} - \frac{1}{\tau_{90K}}\right) = -\frac{E_a}{RT} + A$$

where τ_{obs}, τ_{90K}, E_a, R, T, and A are observed emission lifetime at each temperature, emission lifetime at 90 K, activation energy, gas constant, temperature, and frequency factor, respectively.
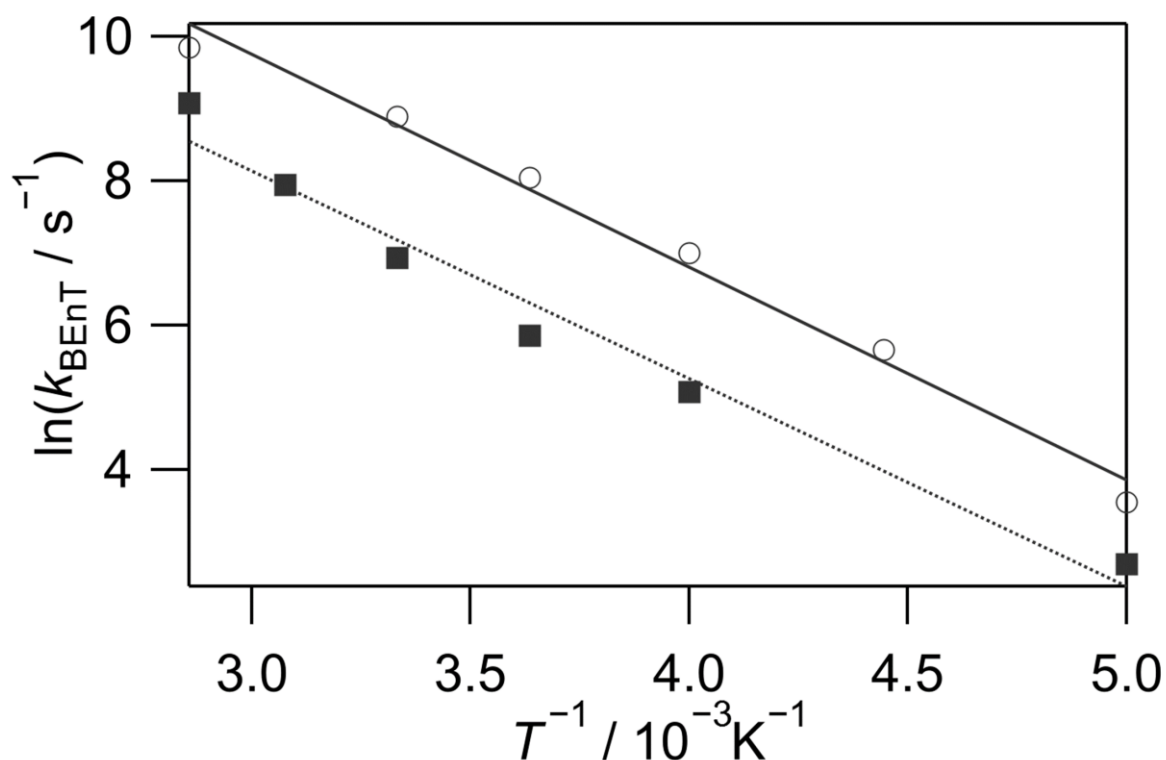
Figure S7. Arrhenius plots and fitting lines for [Tb(hfa)$_3$(tppo)$_2$] (circle and solid line) and [Tb(hfa)$_3$(tcpo)$_2$] (square and dotted line).

Table S10. Arrhenius parameters for [Tb(hfa)$_3$(tppo)$_2$] and [Tb(hfa)$_3$(tcpo)$_2$].

Entry	A / s^{-1}	E_a / cm^{-1}
[Tb(hfa)$_3$(tppo)$_2$]	1.2×10^8	2,000
[Tb(hfa)$_3$(tcpo)$_2$]	1.9×10^7	2,000
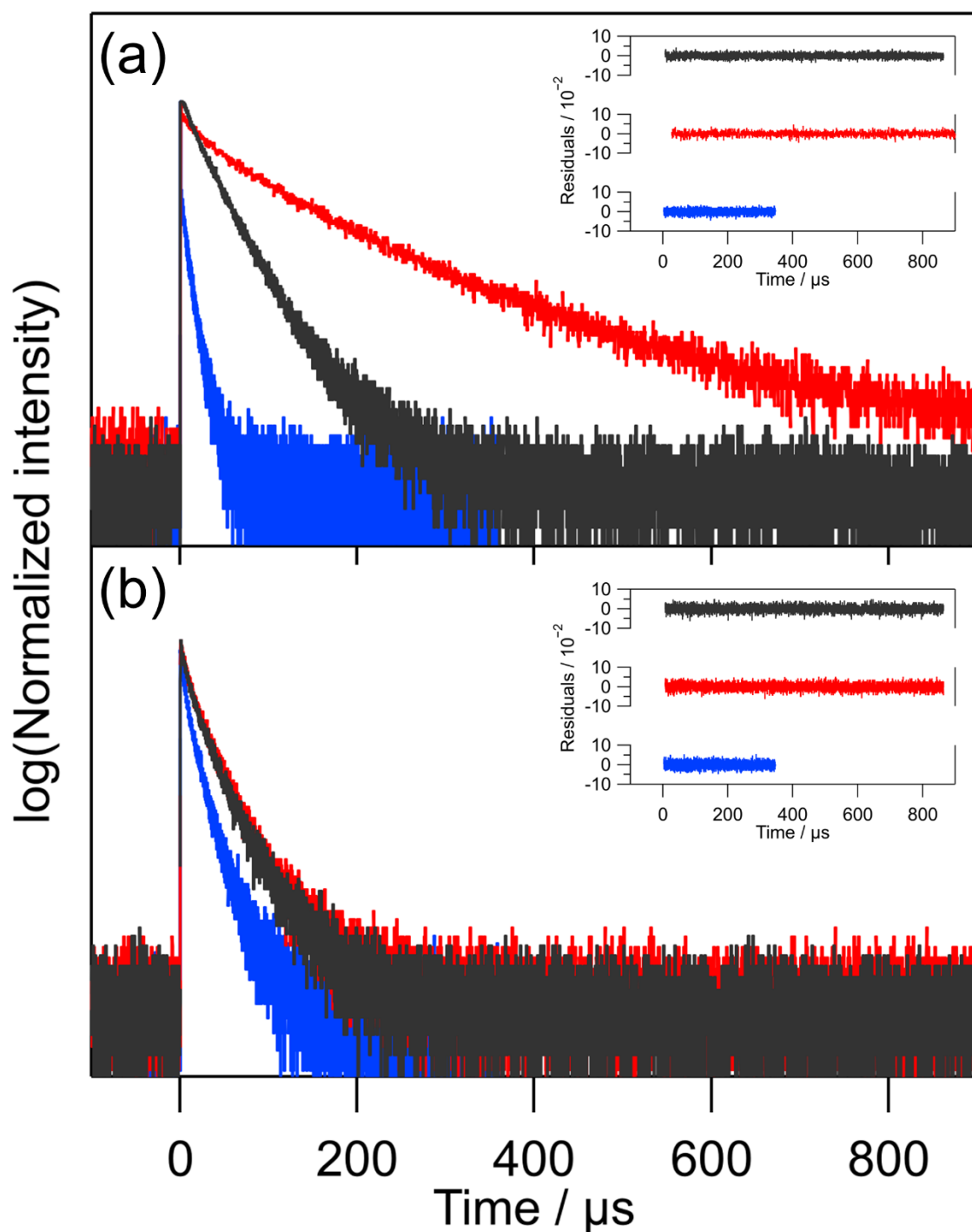
Figure S8. Emission decay curves (λ_{ex} = 355 nm, λ_{em} = 500 nm, 293 K) of (a) [Gd(hfa)$_3$(tppo)$_2$] and (b) [Gd(hfa)$_3$(tcpo)$_2$] under air (black lines), vacuum (red lines), and O$_2$ (blue lines) conditions (Nd:YAG laser). The inset figures represent the residuals of double-exponential fitting (Chi-squared test: [Gd(hfa)$_3$(tppo)$_2$]: χ^2 = 0.88987 (air), 1.22826 (vacuum), 0.937008 (O$_2$); [Gd(hfa)$_3$(tcpo)$_2$]: χ^2 = 1.78777 (air), 2.0778 (vacuum), 1.47211 (O$_2$)).

Table S11. Oxygen-concentration dependent emission lifetimes (λ_{ex} = 355 nm, λ_{em} = 500 nm, 293 K) of [Gd(hfa)$_3$(tppo)$_2$]. The average emission lifetimes were obtained through ten measurements.

Condition	τ_1 / μs	τ_2 / μs	τ_{avg} / μs
air	36 (33%)	77 (67%)	64
vacuum	88 (25%)	287 (75%)	237
O$_2$	11 (40%)	19 (60%)	16

Table S12. Oxygen-concentration dependent emission lifetimes (λ_{ex} = 355 nm, λ_{em} = 500 nm, 293 K) of [Gd(hfa)$_3$(tcpo)$_2$]. The average emission lifetimes were obtained through ten measurements.

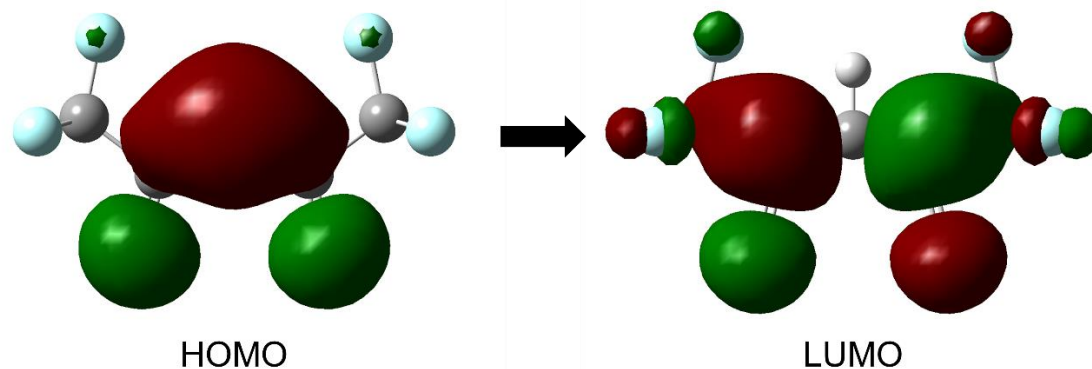| Condition	τ_1 / μs	τ_2 / μs	τ_{avg} / μs
air	22 (26%)	60 (74%)	50
vacuum	26 (31%)	64 (69%)	52
O$_2$	10 (25%)	36 (75%)	29

Quantum chemical calculations

HOMO   LUMO

Figure S9. Molecular orbitals involved in the transition to the T_1 state in hfa ligands (B3LYP / aug-cc-pVDZ). This structure was obtained from DFT calculation (B3LYP / aug-cc-pVDZ).

Table S13. Polarizability of the ligands in [Tb(hfa)₃(tppo)₂] and [Tb(hfa)₃(tcpo)₂].

Entry	Ligand	α / Bohr^3	R / Å	α^2 / Bohr^6	R^{-8} / Å^{-8}	$\Sigma\alpha^2 R^{-8}$ / Bohr^6 Å^{-8}
	hfa1	57.14	2.369[a]	3265	1.008×10^{-3}	
	hfa2	56.95	2.381[a]	3243	9.697×10^{-4}	
	hfa3	57.25	2.399[a]	3278	9.115×10^{-4}	
Tb(hfa)₃(tppo)₂	PO1	180.81	2.271[b]	32692	1.413×10^{-3}	101.4
	PO2	180.90	2.274[b]	32725	1.399×10^{-3}	
	Avg.	106.61	2.339	15041	1.140×10^{-3}	
	hfa1	57.26	2.413[a]	3279	8.700×10^{-4}	
	hfa2	57.38	2.393[a]	3292	9.299×10^{-4}	
	hfa3	57.71	2.414[a]	3330	8.686×10^{-4}	
Tb(hfa)₃(tcpo)₂	PO1	182.64	2.264[b]	33357	1.449×10^{-3}	106.1
	PO2	183.44	2.263[b]	33650	1.454×10^{-3}	
	Avg.	107.69	2.349	15382	1.114×10^{-3}	

ULC-BLYP / cc-pVDZ. The single crystal structures were used for the calculations.

PO: Phosphine oxide ligand.

[a] Average of two Tb-O distances.

[b] Tb-O distance.

**Table S14.** Energy levels and oscillator strengths of LMCT states in [Tb(hfa)$_3$(tppo)$_2$].

	Excited state	λ / nm	E_{CT} / cm^{-1}	f_{CT}	E_{CT}^{-3} / cm^3	$E_{CT}^{-3}f_{CT}$ / cm^3
LMCT1	63	194.95	51295	0.0001	7.41×10^{-15}	7.41×10^{-19}
LMCT2	65	194.40	51440	0.0028	7.35×10^{-15}	2.06×10^{-17}
LMCT3	66	193.26	51744	0.0013	7.22×10^{-15}	9.38×10^{-18}
LMCT4	67	192.30	52002	0.0011	7.11×10^{-15}	7.82×10^{-18}
LMCT5	68	191.37	52255	0.0014	7.01×10^{-15}	9.81×10^{-18}
LMCT6	69	190.90	52383	0.0023	6.96×10^{-15}	1.60×10^{-17}
LMCT7	70	190.42	52515	0.0006	6.90×10^{-15}	4.14×10^{-18}
LMCT8	71	189.47	52779	0.0010	6.80×10^{-15}	6.80×10^{-18}
LMCT9	72	189.11	52879	0.0006	6.76×10^{-15}	4.06×10^{-18}
LMCT10	80	179.45	55726	0.0061	5.78×10^{-15}	3.53×10^{-17}
LMCT11	81	178.73	55950	0.0003	5.71×10^{-15}	1.71×10^{-18}
LMCT12	82	178.48	56029	0.0107	5.69×10^{-15}	6.08×10^{-17}
LMCT13	86	177.79	56246	0.0026	5.62×10^{-15}	1.46×10^{-17}
LMCT14	87	177.61	56303	0.0045	5.60×10^{-15}	2.52×10^{-17}
LMCT15	88	177.12	56459	0.0228	5.56×10^{-15}	1.27×10^{-16}
LMCT16	90	176.72	56587	0.0143	5.52×10^{-15}	7.89×10^{-17}
LMCT17	92	176.24	56741	0.0306	5.47×10^{-15}	1.68×10^{-16}
LMCT18	95	175.75	56899	0.1184	5.43×10^{-15}	6.43×10^{-16}
LMCT19	96	175.73	56905	0.1459	5.43×10^{-15}	7.92×10^{-16}
LMCT20	97	175.66	56928	0.0156	5.42×10^{-15}	8.46×10^{-17}
Avg.		183.77	54503	0.0192	6.24×10^{-15}	1.05×10^{-16}

ULC-BLYP / Stuttgart RSC 1997 for Tb atom, cc-pVDZ for C, H, O, F, and P atoms.

Table S15. Energy levels and oscillator strengths of LMCT states in [Tb(hfa)$_3$(tcpo)$_2$].

	Excited state	λ / nm	E_{CT}/cm^{-1}	f_{CT}	E_{CT}^{-3} / cm^3	$E_{CT}^{-3}f_{CT}$ / cm^3
LMCT1	28	197.82	50551	0.0024	7.74×10^{-15}	1.86×10^{-17}
LMCT2	29	197.64	50597	0.0014	7.72×10^{-15}	1.08×10^{-17}
LMCT3	30	196.72	50834	0.0013	7.61×10^{-15}	9.90×10^{-18}
LMCT4	31	193.93	51565	0.0020	7.29×10^{-15}	1.46×10^{-17}
LMCT5	32	193.42	51701	0.0034	7.24×10^{-15}	2.46×10^{-17}
LMCT6	33	192.75	51881	0.0019	7.16×10^{-15}	1.36×10^{-17}
LMCT7	34	192.31	51999	0.0004	7.11×10^{-15}	2.84×10^{-18}
LMCT8	35	191.76	52149	0.0004	7.05×10^{-15}	2.82×10^{-18}
LMCT9	36	190.39	52524	0.0005	6.90×10^{-15}	3.45×10^{-18}
LMCT10	45	182.20	54885	0.0007	6.05×10^{-15}	4.23×10^{-18}
LMCT11	46	182.00	54945	0.0030	6.03×10^{-15}	1.81×10^{-17}
LMCT12	47	181.04	55236	0.0052	5.93×10^{-15}	3.09×10^{-17}
LMCT13	48	180.49	55405	0.0028	5.88×10^{-15}	1.65×10^{-17}
LMCT14	49	179.80	55617	0.0006	5.81×10^{-15}	3.49×10^{-18}
LMCT15	50	179.16	55816	0.0006	5.75×10^{-15}	3.45×10^{-18}
LMCT16	51	179.11	55832	0.0009	5.75×10^{-15}	5.17×10^{-18}
LMCT17	52	178.69	55963	0.0014	5.71×10^{-15}	7.99×10^{-18}
LMCT18	53	178.48	56029	0.0004	5.69×10^{-15}	2.27×10^{-18}
LMCT19	54	177.63	56297	0.0029	5.60×10^{-15}	1.63×10^{-17}
LMCT20	56	176.92	56523	0.0023	5.54×10^{-15}	1.27×10^{-17}
Avg.		186.11	53817	0.0017	6.48×10^{-15}	1.11×10^{-17}

ULC-BLYP / Stuttgart RSC 1997 for Tb atom, cc-pVDZ for C, H, O, F, and P atoms.
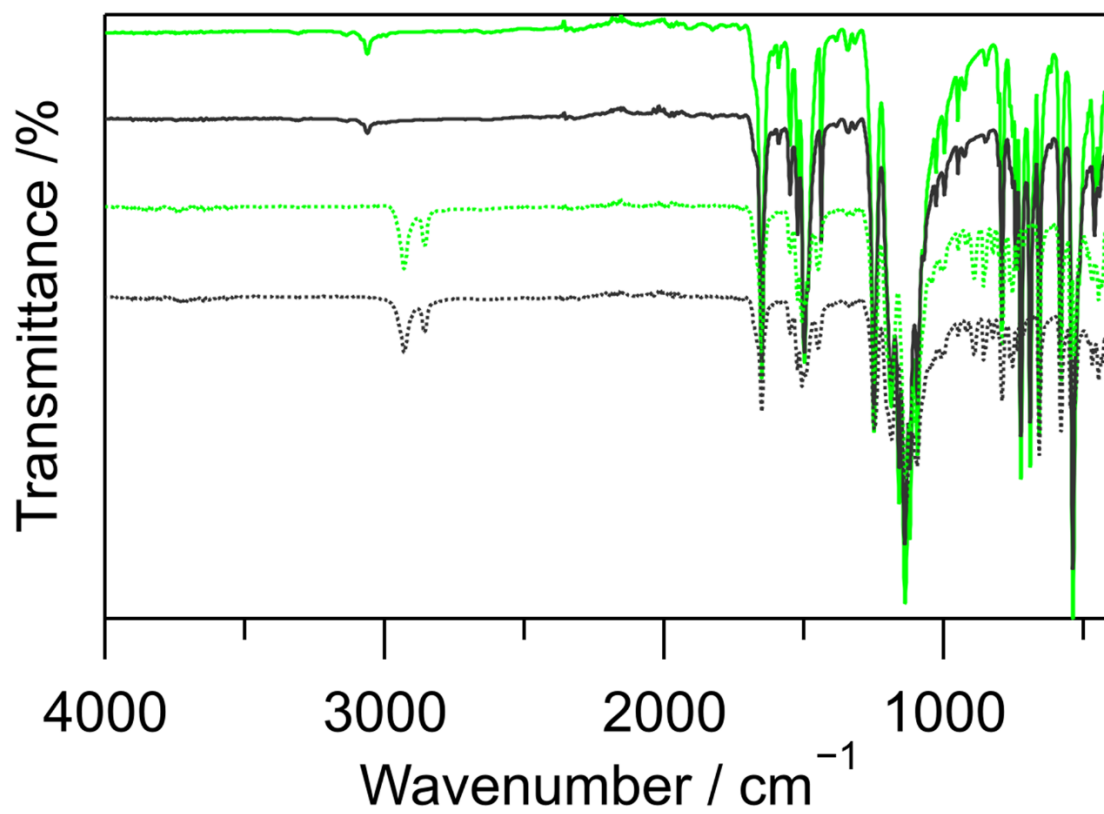
Figure S10. FT-IR spectra of the Tb(III) (green lines) and Gd(III) (black lines) complexes: [Ln(hfa)₃(tppo)₂] (solid lines), [Ln(hfa)₃(tcpo)₂] (dotted lines).
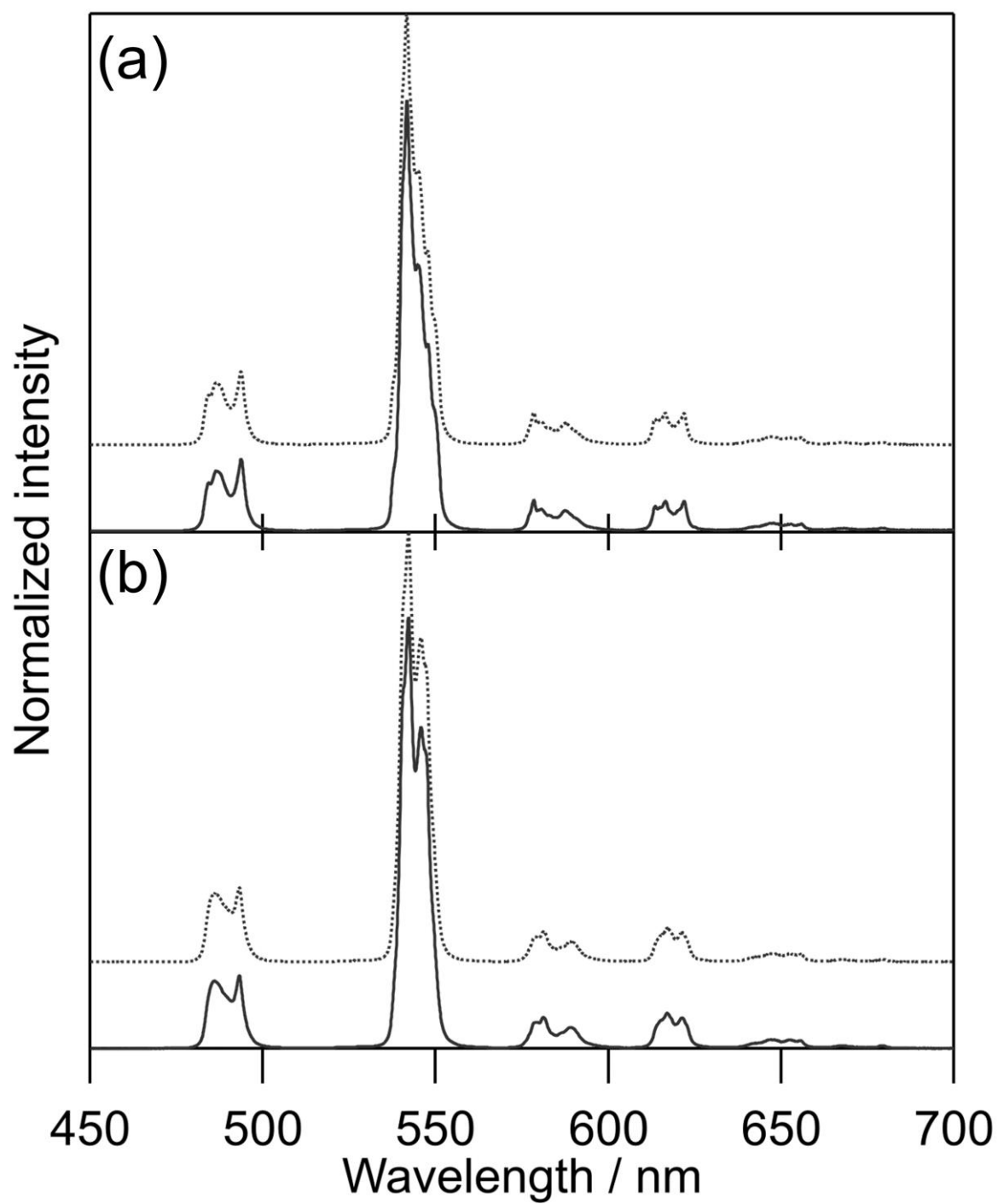
Figure S11. Emission spectra (λ_{ex} = 360 nm, 293 K) of (a) [Tb(hfa)₃(tppo)₂] and (b) [Tb(hfa)₃(tcpo)₂] in air (dotted lines) and under vacuum (solid lines).

References

1. David Casanova, Miquel Llunell, Pere Alemany, and Santiago Alvarez, *Chem. Eur. J.*, 2005, **11**, 1479–1494.

2. Mark Pinsky and David Avnir, *Inorg. Chem.*, 1998, **37**, 5575–5582.

3. SHAPE, version 2.1. Continuous shape measures calculations. Electronic Structure Group, Universitat de Barcelona: Spain (2010).

4. J. C. G. Bünzli and S. V. Eliseeva, Basics of lanthanide photophysics, *Lanthanide Luminescence*, P. Hänninen and H. Härmä, Springer Berlin Heidelberg, 2010, vol. 7, 1–45.